Introduction to Rain and Fog Attenuation on Automotive Surround Sensors

Sinan Hasirlioglu
CARISSMA
Technische Hochschule Ingolstadt, 85049, Germany
Johannes Kepler University Linz, 4040, Austria
Email: sinan.hasirlioglu@thi.de

Andreas Riener
CARISSMA
Technische Hochschule Ingolstadt, 85049, Germany
Johannes Kepler University Linz, 4040, Austria
Email: andreas.riener@thi.de

***Abstract*—Surround sensors in automated vehicles use electromagnetic waves to perceive their local environment. Due to atmospheric phenomena such as rain and fog, the waves are attenuated and limit sensor performance. As already small errors in sensor data measurements could lead to severe accidents, involved sensors should be able to detect measurement errors caused by adverse weather conditions and react accordingly. Rain drops as well as fog drops absorb and scatter electromagnetic waves depending on different properties. Studying the interaction of electromagnetic waves and hydrometeors has a long history in meteorology and radio engineering. This paper gives an overview of the basic knowledge with focus on automotive applications. We focus on camera, lidar, and radar sensors and describe the attenuation in visible, near infrared, and millimeter frequency ranges. For simulating automotive sensors, different disturbance models must be developed for each sensor type. This work should serve as a quick introduction to the field of rain and fog attenuation, highlights potential problems, and discusses possible solutions.**

I. Introduction

The WHO Global Health Observatory data indicates that over 1.25 million people die in traffic accidents annually [1]. To save lives, car manufacturers spend lot of efforts on the development of safety systems and automated driving functions, which are based on data from surround sensors. As small errors in sensor data measurements could lead to severe accidents with major injuries or traffic fatalities, it is of utmost importance to ensure high reliability and accuracy.

The performance of surround sensors depends on the ambient atmosphere. Electromagnetic waves interact with atmospheric gases such as H_2O, CO_2, O_2 and O_3. In rainy or foggy conditions, the water droplets also absorb and scatter electromagnetic waves, leading to further signal attenuation and reduction of the system reliability.

The authors in [2], [3], and [4] investigated experimentally the influence of rain and fog on automotive surround sensors based on indoor tests. It is shown that rain and fog have direct negative influences on signal strength and contrast. However, radar sensors are robust under foggy conditions, whilst lidar and camera sensors reach their critical point.

Kutila et al. presented in [5] a method for detecting degraded sensor performance depending on the actual outdoor condition. Vehicles should use the most reliable sensor data by reducing the weighting of sensors with degraded performance.

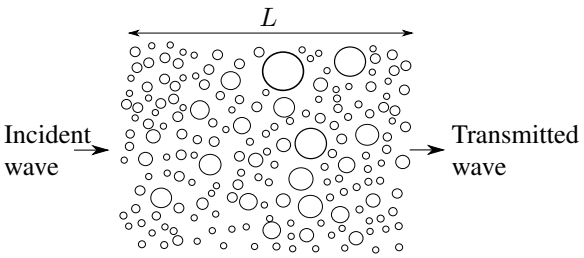

Fig. 1. Electromagnetic wave incident on a volume of spherical uniformly distributed water drops.

Rain consists of water drops with varying numbers, sizes and fall speeds. Typically, the volume of $1\,\mathrm{m}^{-3}$ of air contains about 10^3 raindrops with more small drops than large ones. Small raindrops are close to spherical, whereas larger drops become oblate spheroidal and resembles a hamburger bun [6]. Due to this, the raindrops can be characterized by their equivolume diameter. The diameter ranges between 0.1 and 6 mm and the fall speeds vary from 0.1 to greater than 9 m/s.

Fog is present, when water droplets suspended in the air decrease the visibility to less than 1 km. The diameter of fog droplets ranges from 5 to 20 µm and depends on fog type [7]. Advection fog is coastal fog and is caused by horizontal movement of warm air mass over cold water with average diameter in the order of 20 µm. Radiation fog is caused by cooling of air over night and is characterized by smaller drops.

The fundamental research in this field was published by Ryde in the early 1940's. The author calculated the electromagnetic cross sections of spherical raindrops and used physical parameters of rain in order to derive the relation between rainfall rate and attenuation.

Outline

This paper is organized as follows. Section II gives an overview about the interaction between electromagnetic waves and hydrometeors, section III describes the characteristics of rain and fog. Further on, section IV describes the specific attenuation due to the influence of rain and fog. Finally, section V summarizes the results and the contribution of this paper.

978-1-5386-1526-3/17/$31.00 ©2017 IEEE

II. Interaction between electromagnetic waves and hydrometeors

Scattering and absorption of radiation by particles is a well-developed field of physics. For a more detailed discussion we refer the reader to [7], [8] and [9]. Scattering of electromagnetic waves by particles is the process, where the direction of the incident wave is changed by a particle. Absorption is the process, where heat energy is produced. Both, scattering and absorption, extract energy from the incident wave and are named extinction.

Maxwell's equations are the basis of theoretical and computational methods describing the interaction of electromagnetic waves with particles. The exact solutions to Maxwell's equations are only known for selected geometries. Numerical methods such as Seperation of Variables Method are discussed in [10] and will not be discussed further in this paper.

Scattering depends on the ratio between the wavelength λ of the incident wave and the size of the particle, expressed by the radius r. Therefore, the size parameter x is defined as

$$x = \frac{2\pi r}{\lambda}. \tag{1}$$

Camera sensors are passive sensors and measure the electromagnetic wave from the sun in the visible wavelength range. Lidar sensors are active sensors and operate normally in the near infrared range. Radar sensors are also active sensors and use millimeter waves for the environment detection.

Different types of scattering are used depending on the size parameter x. If the particle is very small compared to the wavelength ($x \ll 1$), the Rayleigh scattering is used. Mie theory is used if the particle is comparable equal to the wavelength ($x \approx 1$). If the wavelength is small compared to the particle size ($x \gg 1$), the scattering for large particle approximates the laws of geometric optics.

Table I shows the size parameters for each surround sensor type. For camera sensors, the mean wavelength is approximated to 550 nm. Lidar sensors emit laser light usually with the wavelength of 905 nm. Radar sensors (far field) transmit electromagnetic waves with a wavelength of 3.9 mm. The average raindrop radius is approximated to 0.5 mm, whereas, the fog drop radius is approximated to 5 µm. The difference between the drop sizes is in the order of 10^2 - 10^3.

TABLE I
Size parameter values for each sensor type.

	Camera (550 nm)	Lidar (905 nm)	Radar (3.9 mm)
Rain drop ($r = 0.5$ mm)	5712	3471	1
Fog drop ($r = 5$ µm)	57	35	0.008

It can be seen that the size parameters of camera sensors are not significantly different from lidar sensors. For scattering with rain drops, geometric optics can be used. Interactions with fog drops can be calculated by Mie's theory. For radar sensors, the size parameter differ greatly from lidar and camera sensors. For interactions with rain drops, Mie's theory can be used. Fog drops are small compared to the wavelength, which can be calculated by Rayleigh scattering.

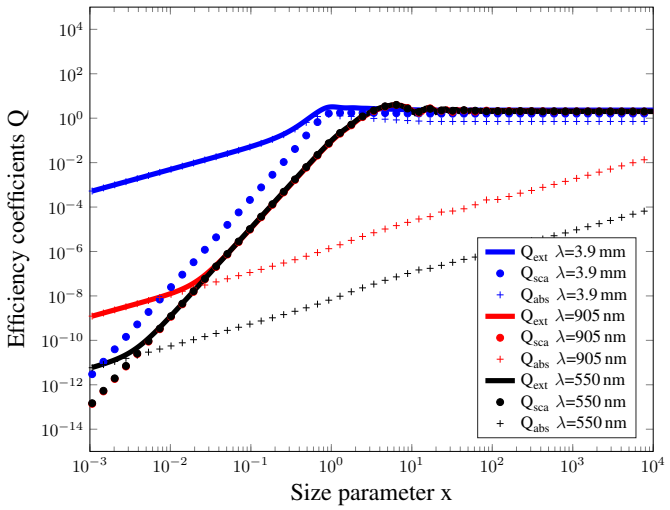

Fig. 2. Efficiency coefficients of electromagnetic waves at millimeter, near infrared and visible wavelengths as a function of size parameter. The calculations are performed by using the simulation software MiePlot [11].

Rayleigh scattering and Mie theory use the concept of cross sections C_{ext}, C_{sca} and C_{abs}, which indicates the area interacting with the particles. It is the ratio of the absorbed or scattered power to the incident power density. The extinction cross section is the sum of scattering and absorption cross section. Furthermore, the cross sections have the dimension of area while the efficiency coefficients Q_{ext}, Q_{sca} and Q_{abs} are normalized cross sections which can be calculated by

$$Q_{ext} = \frac{C_{ext}}{\pi r^2} \tag{2}$$

and are consequently dimensionless.

Fig. 2 shows the efficiency coefficients Q_{ext}, Q_{sca} and Q_{abs} for the different sensor types. The calculations are performed by using the computer simulation software MiePlot [11]. It can also produce graphs of scattered intensity as a function of r, λ, scattering angle θ and refractive index m.

It can be seen, that with increasing size parameter x the graphs of Q_{ext} are increasing and asymptotes the value 2, which is called extinction paradox [7].

The blue graphs represent the efficiency coefficients for extinction, scattering and absorption of long range radar sensors (see Table I). The linear area approximately up to $x = 0.1$ is the Rayleigh region. Further, the area approximately up to $x = 10$ is the Mie region. For small size parameters (and thus small drop sizes), absorption predominates. Scattering becomes relevant for size parameters greater than 1.

The red and black graphs represent the efficiency coefficients for camera and lidar. The border between Rayleigh and Mie region is approximately at $x = 1$ and the border between Mie and optical region is at $x = 100$. It can be inferred that extinction efficiency is more close to absorption for small x, while it approaches the scattering efficiency in the Mie and optical regions.

The main differences between radar and the other surround sensors can be explained by the complex refractive index m of water, which is wavelength and temperature dependent and given by

$$m = n - in' \tag{3}$$

where the real part indicates the phase velocity and the imaginary part the strength of absorption loss of electromagnetic waves. Fig. 3 illustrates the complex refractive index of water as a function of frequency, given by Segelstein [12]. The first solid line highlights the frequency of radar sensors and the second solid line the frequency of lidar sensors. The dotted lines indicate the limits of visible light spectrum. It can be seen that the imaginary part of the refractive index can be neglected in visible and near infrared spectrum. Millimeter waves are strongly affected by absorption effects. It can therefore be concluded that water, covering the radar sensor, has adverse impacts on the perception of the environment.

A. Rayleigh Scattering

Rayleigh scattering occurs when the diameter of the particles is much smaller than the wavelength of the incident electromagnetic wave. If we assume that the dielectric constant of the ambient medium is one, we can calculate the scattering efficiency as

$$Q_{sca} = \frac{8}{3}x^4 \left| \frac{m^2 - 1}{m^2 + 2} \right|^2 \tag{4}$$

and absorption efficiency as

$$Q_{abs} = -4xIm(\frac{m^2 - 1}{m^2 + 2}) \tag{5}$$

where x is the size parameter and m the complex refractive index. The most significant factor is the λ^{-4} dependence (if we substitute Eq. 1 into Eq. 4) which means, that shorter wavelengths scatter more strongly than longer wavelengths. For example, blue light scatters much more than near infrared light, which is responsible for the blue sky. It can be seen in Fig. 2, that the scattering efficiency factor of camera (black dotted line) is higher than those of lidar (red dotted line). Furthermore, the incoming wave is scattered equally in the forward and backward direction.

B. Mie Theory

Mie scattering takes place when the particle size is similar to the wavelength of the incident electromagnetic wave. The theory was developed by Gustav Mie in 1908 [13]. The Mie theory applies the boundary conditions which describe scattering and absorption of electromagnetic radiation by spherical and homogeneous particles. The Mie efficiency for extinction is given as

$$Q_{ext} = \frac{2}{x^2} \sum_{k=1}^{k_{max}} (2n+1) Re[a_n + b_n] \tag{6}$$

where a_n and b_n are Mie coefficients, which depend on x and on the complex refractive index and are calculated using Bessel and Hankel functions. To avoid the infinity series the index value is truncated by $k_{max} = x + 4x^{1/3} + 2$, given by [14]. When the radius is decreased, the forward and backward scattering distributions become essentially symmetric and approach the Rayleigh scattering solution. As the particle radius increases with respect to the wavelength, forward direction is larger than the reverse direction and approaches the geometric optics. Generally, the single scattering properties can be calculated by using Mie theory for spheres of any size, but the Mie solutions are expansions in terms of the size parameter x. Numerous complex terms are needed to obtain converged solutions for large values of x. For this reason, available Mie codes can be used for limited x values (approx. 20000).

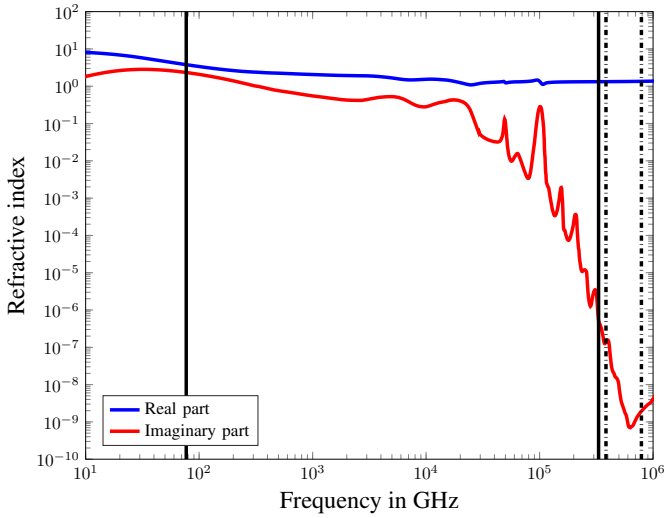

Fig. 3. Complex refractive index of water as a function of frequency [12]. The real part indicates the phase velocity and the imaginary part the strength of absorption loss of electromagnetic waves. The first solid line highlights the frequency of long range radar sensors and the second solid line the frequency of lidar sensors. The dotted lines indicate the limits of visible light spectrum.

C. Geometric Optics

Interactions of electromagnetic waves with particles much larger than the incident wavelength can be approached by geometric optics (ray tracing), which depends on size and refractive index, and diffraction, which depends on shape and size but is independent of the refractive index.

Van de Hulst presented in [7] a combination of geometrical optics and Huygen's principle as

$$Q_{ext} = 2 - 4e^{-p\tan\beta}\left(\frac{\cos\beta}{\rho}\right)\sin(\rho-\beta) - 4e^{-p\tan\beta}\left(\frac{\cos\beta}{\rho}\right)^2\cos(\rho-2\beta) + 4\left(\frac{\cos\beta}{\rho}\right)^2\cos(2\beta) \tag{7}$$

where

$$\rho = 2x(n-1), \qquad \tan\beta = \frac{n'}{n-1}$$

and x the size parameter. n and n' are the real and imaginary parts of the complex refractive index m. It is assumed that $n-1$ and n' are $<<1$ and $x >>1$.

The physical processes of geometric optics include reflected and refracted rays. Refracted rays may be absorbed inside the particle or being internally reflected several times. The energy of reflected and refracted rays can be calculated by Fresnel's and Snell's laws and contribute to total scattering by the particle. Non-absorptive particles scatter the wave up to 99.5% of the total forward scattering from externally reflections and refractions with no internal reflections [7].

Large particles also scatter waves passing by the particle, known as diffraction, which is concentrated in a narrow lobe around forward direction. Like geometric optics, diffraction contains an amount of energy equal to the incident wave. In far field (much greater than the particle size), the diffracted wave can be approximated by Fraunhofer diffraction theory. More detailed information can be found in [15], where the authors showed that geometrics optics and Mie theory are in agreement for $x \geq 400$.

III. Rain and Fog Characteristics

For the characterization of rain and fog scenarios, different models have been developed in the past. Regarding the drop size distribution, namely exponential, gamma, lognormal, and Weibull are used for characterizing rain and fog.

The most widely used distribution is presented by Marshall and Palmer in [16], a one parameter exponential distribution of the form

$$N(D) = N_0 e^{-\Lambda D} \tag{8}$$

where $N(D)$ is the concentration of raindrops between D and $D+dD$, N_0 the intercept parameter and Λ the slope parameter. They proposed a simple parametrization as a function of rain intensity R with N_0 = 8000 in $\mathrm{m}^{-3}\mathrm{mm}^{-1}$ and Λ = 4.1 $\mathrm{R}^{-0.21}$ in mm^{-1}. Joss et al. proposed in [17] values for different types of rainfall, such as drizzle, widespread rain and thunderstorm. Sekhorn and Srivastava proposed an exponential model, where the intercept parameter depends on the rain intensity [18]. The fit of this curve is not appropriate for small drop diameters which contribute a major part to the rain attenuation. Furthermore, the model fails to fit the rain drop distribution in short sampling times. However, the distribution tends to be exponential when many distributions from different conditions are summarized. Therefore, the model is appropriate in applications where an average over time and/or space is taken into account [19].

Many researchers (e.g. Deimendjan [20], Ulbrich [21]) have proposed the use of the modified gamma distribution as

$$N(D) = N_0 D^{\mu} e^{-\Lambda D} \tag{9}$$

with three parameters N_0, Λ and μ. The gamma distribution is a generalization of the exponential form found by Marshall and Palmer and is equal to it if μ = 0. A disadvantage of this model is that the intercept parameter N_0 is not a physical quantity. Testud et al. presented in [22] a mathematical technique to normalize rain spectra and identify the shape of the distribution.

Feingold and Levin proposed in [23] another three-parameter lognormal distribution which is given by

$$N(D) = \frac{N_T}{\sqrt{2\pi}\ln(\sigma)D} \exp\left(\frac{-\ln^2(D/D_g)}{2\ln^2(\sigma)}\right) \tag{10}$$

where N_T is the total drop number per unit volume in m^3, D_g the geometric mean diameter in mm and σ the standard geometrical deviation of D. All three parameters have physical meaning. Further, all the moments of the distribution are themselves lognormally distributed and used to determine the parameters. Similar model was proposed by Markowitz in [24].

Empirical relations of the general behavior as a function of rain intensity R are given by following approximations.

$$\sigma = 1.43 - 3 \cdot 10^{-4} R \tag{11}$$

$$N_T = 172 R^{0.22} \tag{12}$$

$$D_g = 0.72 R^{0.23} \tag{13}$$

The Weibull raindrop-size distribution was firstly proposed by Sekine and Lind in [25] as

$$N(D) = N_0 \frac{c}{b} \left(\frac{D}{b}\right)^{c-1} e^{-\left(\frac{D}{b}\right)^c} \tag{14}$$

where N_0=1000 $\mathrm{m}^{-3}\mathrm{mm}^{-1}$, c = 0.95 $R^{0.14}$ and b = 0.26 $R^{0.44}$. The calculation of rain attenuation showed good agreement with measurements of millimeter waves.

It is interesting that with increasing rain intensity, the median volume diameter remains constant and does not increase in size. It even tends to decrease at high intensities [26]. Smith et al. presented in [27] the variability of rain intensity and drop distribution in heavy rain scenarios based on the parameters of a gamma distribution model. They showed a large temporal variability based on storm periods.

With given drop size distribution, several quantities describing the precipitation can be estimated. The physical moment M_k in $\mathrm{mm}^k\mathrm{m}^{-3}$ result from the integration

$$M_k = \int_0^{\infty} N(D) D^k dD \tag{15}$$

where, for example, D^6 is used for radar reflectivity, D^3 for volume of water and D^2 for the calculation of the attenuation. The radar reflectivity factor Z in $\mathrm{mm}^6\mathrm{m}^{-3}$ at wavelengths where the Rayleigh approximation is valid is given by

$$Z = \int_0^{\infty} N(D) D^6 dD \tag{16}$$

and the rain intensity R in mm/h is estimated by

$$R = \frac{6\pi}{10^4} \int_0^{\infty} N(D) D^3 v(D) dD \tag{17}$$

where $v(D)$ is the terminal fall speed of the raindrop in m/s. The calculation of the attenuation is presented in section IV.

Similar to rain, fog is also characterized by it's drop size distribution. One of the most used distribution is, besides the above-mentioned, the Best's formula [28].

However, fog is further characterized by it's water content (g/m^3), visibility, and temperature. Visibility is a simple and direct parameter defined as the distance to an object where a light beam with the wavelength $\lambda = 550$ nm is attenuated to 2% of its origin power [29]. Fog is present when the visibility of the scene decreases to less than 1 km and the relative humidity of the ambient atmosphere reaches saturation level [30]. Some fog banks are more dense than others, because droplets can absorb more water and grow in size. Very dense fog are defined as visibility reduced to less than 50 m.

The liquid water content W in g/m^3 is given by

$$W = \frac{\pi}{6}\rho_w \int N(D)D^3 dD \tag{18}$$

where ρ_w is the water density and D the water drop diameter.

Eldridge's empirical relationship between visibility V and liquid water content W is described as

$$V = 0.024W^{-0.65} \tag{19}$$

for radiation fog, where the drop diameters are $< 10\,\mu$m. For advection fog, the author recommends that the coefficient 0.024 be replaced by 0.017 [31].

IV. Rain and Fog Attenuation

Determining the specific attenuation on electromagnetic waves is based on three assumptions. First, the contribution of each drop is additive and independent of other drops. Second, the drops are assumed to be spherical water drops, which scatter and absorb energy from the incident wave. Finally, the intensity of the wave decays exponentially as it propagates through the volume of rain or fog.

If an electromagnetic wave with transmitted power P_t is incident on a volume of uniformly distributed spherical water drops with diameters D and extended over a length L, the received power P_r decays according to the law of Beer-Lambert

$$P_r = P_t e^{-\gamma_{ext} L} \tag{20}$$

where γ_{ext} is the extinction coefficient in 1/length for the volume of water drops. The specific attenuation α in dB/km is expressed as a positive decibel value given by

$$\alpha = 10 \log_{10}(\frac{P_t}{P_r}) \tag{21}$$

Converting the log to the base e by substituting Eq. 20 into Eq. 21 it results

$$\alpha = 4.434 \gamma_{ext} L. \tag{22}$$

The extinction coefficient γ_{ext} is expressed as

$$\gamma_{ext} = NC_{ext} = NQ_{ext} r^2 \pi = NQ_{ext} D^2 \frac{\pi}{4} \tag{23}$$

where N is the number of drops per unit volume and Q_{ext} the extinction efficiency factor [7]. As already mentioned, Q_{ext} is the sum of scattering efficiency Q_{sca} and absorption efficiency Q_{abs} (see Fig. 2).

If the rain drops have different sizes (drop size distribution), with $N(D)dD$ particles with diameter between D and $D + dD$ per unit volume, then the extinction coefficient must be determined by integrating over all drop sizes expressed as

$$\gamma_{ext} = \frac{\pi}{4} \int_0^\infty N(D) Q_{ext} D^2 dD. \tag{24}$$

The specific attenuation for $L = 1$ km can be calculated by substituting Eq. 24 into Eq. 22 as

$$\alpha = 4.343 \frac{\pi}{4} \int_0^\infty N(D) Q_{ext} D^2 dD. \tag{25}$$

The total specific attenuation α_t in dB is then obtained by integrating the specific attenuation over the total path L

$$\alpha_t = 4.343 \frac{\pi}{4} \int_0^L \left[\int_0^\infty N(D) Q_{ext} D^2 dD \right] dL \tag{26}$$

where the integration over L is taken over the extent of the rain volume in the direction of propagation. This is necessary due to the varying drop distribution $N(D)$ along the path. This variability must be considered in the calculations. For the development of useful rain attenuation prediction models, the variability can be approximated statistically [32]. It can be seen in Eq. 26, that the total specific attenuation depends on the characteristics of rain or fog, number of drops and drop sizes, and the extinction efficiency which is temperature and frequency dependent.

Using Eq. 25, which assumes a length L of 1 km, the specific attenuation can be calculated as a function of frequency. For the rain drop size distribution $N(D)$ the Eq. 10 - 13 are used. The drop size distribution of dense continental fog is based on the modified gamma distribution parameters of Harris, which can be found in [33]. The efficiency coefficients Q_{ext} at frequencies 10 to 10^6 GHz are calculated by using the computer simulation software MiePlot [11]. The resultant graphs of the specific attenuation can be seen on the left side of Fig. 4.

The specific attenuation due to rain increases with the frequency, with a maximum at 50-200 GHz region, after which it remains relatively constant. It is clear, that at a frequency of 77 GHz (long range radar) the losses due to rain are much greater than compared to fog. Short range radars (24 GHz) are less attenuated by rain and fog and already used for driver assistant systems. The rain attenuation in visible and infrared frequency range are in the constant region and in the same order of magnitude as long range radars.

Regarding fog influence, it can be seen that radar sensors are much more robust. For lidar sensors, as well as camera sensors, the specific attenuation reaches values over 100 db/km. Therefore, surround sensors operating at optical and near infrared wavelengths are not recommendable for environment detection and vehicle control under foggy conditions. It can lead to a total failure of the sensor. Longer wavelengths, such as millimeter waves, show lower attenuation.

The calculated specific attenuation can be compared with literature. The right side of Fig. 4 shows the specific attenuation of rain and fog as a function of frequency, which can be found in [34]. The minor differences can be explained

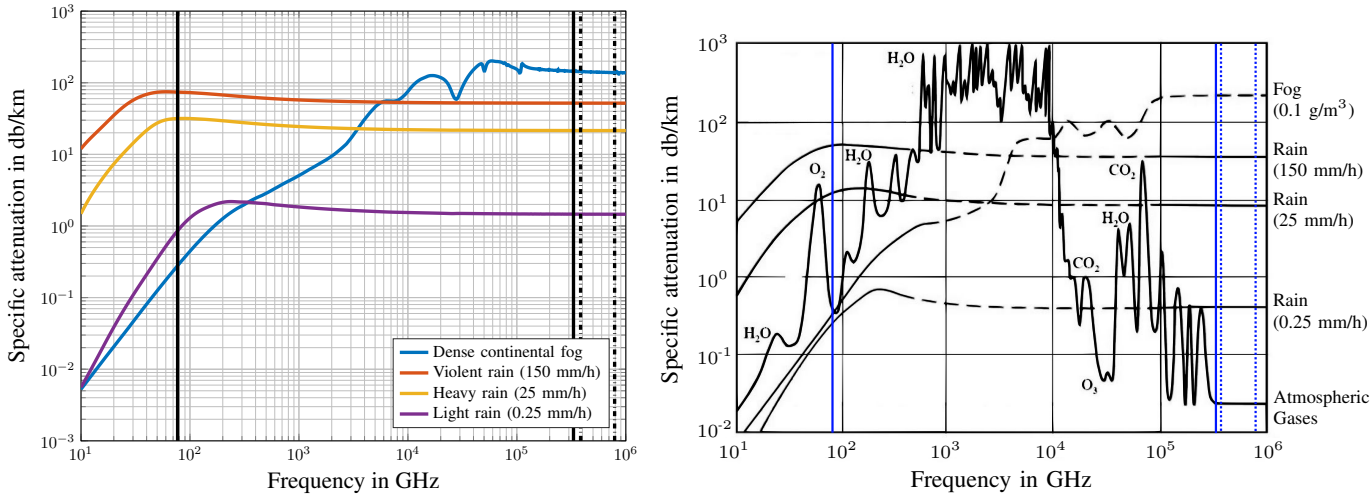

Fig. 4. Left: Calculated specific attenuation as a function of frequency by using lognormal distribution for rain [23] and modified gamma distribution for dense continental fog [33]. The efficiency coefficients Q_{ext} are calculated by using the software MiePlot [11]. Right: Specific attenuation according to [34]. The first vertical solid line in each plot highlights the frequency of long range radar sensors and the second solid line the frequency of lidar sensors. The dotted lines indicate the visible light spectrum.

by different drop size distributions. However, the robustness of radar sensors in foggy conditions and similar behavior of all surround sensors in heavy rain conditions are hereby confirmed. It is also clear, that optical and near infrared wavelengths are strongly attenuated in foggy conditions.

The specific attenuation due to clear atmospheric gases at 20°C, one atmosphere pressure and 7.5 g/m^3 water vapor can also be seen on the right side of Fig. 4 [35]. The molecular absorption differs depending on the frequency of the electromagnetic wave. At lower frequencies, for example 24 GHz, the attenuation is relatively low (<1 dB/km). At millimeter wavelengths, the main attenuation is caused by H_2O and O_2. The window between 70 and 90 GHz show low molecular attenuation and is therefore used for long range radar systems. The molecular absorption at near infrared and optical wavelengths is caused by CO_2 and are very low, compared to millimeter wavelengths.

The ITU-R recommends for the calculation of the attenuation the use of the power law relationship for rain, which can be approximated by

$$\alpha = aR^b \tag{27}$$

where R is the rain rate in mm/h and a, and b the frequency and temperature dependent constants [36]. For fog attenuation [37], they recommend following equation

$$\alpha = K_l W \tag{28}$$

where K_l is the specific attenuation coefficient in (dB/km)/(g/m^3) and W the liquid water content in g/m^3.

For fog conditions, the Kruse model predicts the specific attenuation in dB/km using the local visibility and is given by

$$\alpha = \frac{3.91}{V}\left(\frac{\lambda}{\lambda_0}\right)^{-q} \tag{29}$$

where V is the visibility in km, λ the wavelength in nm, λ_0 the visibility reference wavelength (550 nm), and q the coefficient related to particle size distribution in the atmosphere. q depends on the visibility and can be calculated as follows

$$q = 0.585V^{\frac{1}{3}} \text{ for } V < 6\,\text{km}. \tag{30}$$

Hence, with increasing wavelength λ the attenuation decreases. Kim modified the Kruse model to improve the match to attenuation at low visibilities to

$$q = 0 \text{ for } V < 0.5\,\text{km} \tag{31}$$

which can be found in [38]. Al Naboulsi et al. presented in [39] a new approach, where advection fog and radiation fog are modeled separately.

Note that the total path attenuation can be determined by adding the attenuation of rain and/or fog to the attenuation due to atmospheric gases and spreading loss, as well as attenuations due to other processes such as cross polarization. A short overview about further attenuation processes can be found in [40]. Non-spherical rain drops lead to attenuation that depends on the polarization of the electromagnetic wave [41].

V. Conclusion

Automated vehicles are equipped with surround sensors, which use electromagnetic waves, to perceive their local environment. It is well known that electromagnetic waves suffer much attenuation while propagating through the atmosphere. In adverse weather conditions, such as rain and fog, the attenuation is increased due to the additional large water particles in the air. Rain drops, as well as fog drops, absorb and scatter electromagnetic waves, leading to a reduction of the system reliability. To enable virtual testing or design more robust sensors, this disturbances must be understood.

This paper gives an overview about the interaction of electromagnetic waves and hydrometeors. Automotive surround sensors such as camera, lidar, and radar operate at different frequency ranges. Based on Rayleigh scattering, Mie theory, and

geometric optics the extinction efficiency can be determined in visible, infrared, and millimeter frequency range. Using the extinction efficiency, the specific attenuation can be calculated with known physical characteristics of rain and fog. It is shown that the rain and fog attenuation, calculated by using the equations in this paper, correspond to literature. Radar sensor radiation penetrate more effective through suspended water in the air, especially under foggy conditions. Camera and lidar sensors are strongly influenced by fog. However, due to the advantages of lidar and camera sensors regarding object classification and tracking, the sensors are essential for automated safety systems. Therefore, it is advisable to detect degraded sensor performance depending on the outdoor condition. Vehicles should use the most reliable sensor data by reducing the weighting of sensors with degraded performance. This work can help to get a quick introduction to the field of rain and fog attenuation on automotive sensor systems.

ACKNOWLEDGMENT

This work is supported under the FH-Impuls program of the German Federal Ministry of Education and Research (BMBF) under Grant No. 13FH7I01IA.

REFERENCES

[1] World Health Organization, *Global status report on road safety 2015*. Geneva, Switzerland: World Health Organization, 2015.

[2] S. Hasirlioglu, I. Doric, C. Lauerer, and T. Brandmeier, "Modeling and simulation of rain for the test of automotive sensor systems," in *2016 IEEE Intelligent Vehicles Symposium (IV)*, pp. 286–291.

[3] S. Hasirlioglu, A. Kamann, I. Doric, and T. Brandmeier, "Test methodology for rain influence on automotive surround sensors," in *2016 IEEE 19th International Conference on Intelligent Transportation Systems (ITSC)*, pp. 2242–2247.

[4] S. Hasirlioglu, I. Doric, A. Kamann, and A. Riener, "Reproducible fog simulation for testing automotive surround sensors," in *2017 IEEE 85th Vehicular Technology Conference*.

[5] M. Kutila, P. Pyykonen, W. Ritter, O. Sawade, and B. Schaufele, "Automotive lidar sensor development scenarios for harsh weather conditions," in *2016 IEEE 19th International Conference on Intelligent Transportation Systems (ITSC)*, pp. 265–270.

[6] L. W. Li, P. S. Kooi, M. S. Leong, and T. S. Yeo, "On the simplified expression of realistic raindrop shapes," *Microwave and Optical Technology Letters*, vol. 7, no. 4, pp. 201–205, 1994.

[7] H. C. Hulst, *Light Scattering by Small Particles*, ser. Dover Books on Physics. Newburyport: Dover Publications, 2012.

[8] S. M. Kulpa and E. A. Brown, *Near-Millimeter Wave Technology Base Study: Volume I. Propagation and Target/Background Characteristics*. Ft. Belvoir: Defense Technical Information Center, 1979.

[9] T. S. Chu and D. C. Hogg, "Effects of precipitation on propagation at 0.63, 3.5, and 10.6 microns," *Bell System Technical Journal*, vol. 47, no. 5, pp. 723–759, 1968.

[10] F. Kahnert, "Numerical methods in electromagnetic scattering theory," *Journal of Quantitative Spectroscopy and Radiative Transfer*, vol. 79-80, pp. 775–824, 2003.

[11] P. Laven, "Simulation of rainbows, coronas, and glories by use of mie theory," *Applied Optics*, vol. 42, no. 3, p. 436, 2003.

[12] D. J. Segelstein, *The complex refractive index of water*, 1981.

[13] G. Mie, "Beiträge zur optik trüber medien, speziell kolloidaler metallösungen," *Annalen der Physik*, vol. 330, no. 3, pp. 377–445, 1908.

[14] C. F. Bohren and D. R. Huffman, *Absorption and Scattering of Light by Small Particles*. Weinheim, Germany: Wiley-VCH Verlag GmbH, 1998.

[15] K.-n. Liou and J. E. Hansen, "Intensity and polarization for single scattering by polydisperse spheres: A comparison of ray optics and mie theory," *Journal of the Atmospheric Sciences*, vol. 28, no. 6, pp. 995–1004, 1971.

[16] J. S. Marshall and W. M. K. Palmer, "The distribution of raindrops with size," *Journal of Meteorology*, vol. 5, no. 4, pp. 165–166, 1948.

[17] J. Joss and A. Waldvogel, "Raindrop size distribution and sampling size errors," *Journal of the Atmospheric Sciences*, vol. 26, no. 3, pp. 566–569, 1969.

[18] R. S. Sekhon and R. C. Srivastava, "Doppler radar observations of drop-size distributions in a thunderstorm," *Journal of the Atmospheric Sciences*, vol. 28, no. 6, pp. 983–994, 1971.

[19] J. Joss and E. G. Gori, "Shapes of raindrop size distributions," *Journal of Applied Meteorology*, vol. 17, no. 7, pp. 1054–1061, 1978.

[20] D. Deirmendjian, *Electromagnetic scattering on spherical polydispersions*. New York NY: American Elsevier Publ, 1969.

[21] C. W. Ulbrich, "Natural variations in the analytical form of the raindrop size distribution," *Journal of Climate and Applied Meteorology*, vol. 22, no. 10, pp. 1764–1775, 1983.

[22] J. Testud, S. Oury, R. A. Black, P. Amayenc, and X. Dou, "The concept of "normalized" distribution to describe raindrop spectra: A tool for cloud physics and cloud remote sensing," *Journal of Applied Meteorology*, vol. 40, no. 6, pp. 1118–1140, 2001.

[23] G. Feingold and Z. Levin, "The lognormal fit to raindrop spectra from frontal convective clouds in israel," *Journal of Climate and Applied Meteorology*, vol. 25, no. 10, pp. 1346–1363, 1986.

[24] A. H. Markowitz, "Raindrop size distribution expressions," *Journal of Applied Meteorology*, vol. 15, no. 9, pp. 1029–1031, 1976.

[25] M. Sekine and G. Lind, "Rain attenuation 0f centimeter, millimeter and submillimeter radio waves," in *12th European Microwave Conference, 1982*, pp. 584–589.

[26] D. C. Blanchard and A. T. Spencer, "Experiments on the generation of raindrop-size distributions by drop breakup," *Journal of the Atmospheric Sciences*, vol. 27, no. 1, pp. 101–108, 1970.

[27] J. A. Smith, E. Hui, M. Steiner, M. L. Baeck, W. F. Krajewski, and A. A. Ntelekos, "Variability of rainfall rate and raindrop size distributions in heavy rain," *Water Resources Research*, vol. 45, no. 4, 2009.

[28] A. C. Best, "Drop-size distribution in cloud and fog," *Quarterly Journal of the Royal Meteorological Society*, vol. 77, no. 333, pp. 418–426, 1951.

[29] F. Nadeem, T. Javornik, E. Leitgeb, V. Kvicera, and G. Kandus, "Continental fog attenuation empirical relationship from measured visibility data," *Radioengineering*, 2010.

[30] F. Nadeem and E. Leitgeb, "Dense maritime fog attenuation prediction from measured visibility data," *Radioengineering*, vol. 19, no. 2, pp. 223–227, 2010.

[31] R. G. Eldridge, "Haze and fog aerosol distributions," *Journal of the Atmospheric Sciences*, vol. 23, no. 5, pp. 605–613, 1966.

[32] L. J. Ippolito, "Radio propagation for space communications systems," *Proceedings of the IEEE*, vol. 69, no. 6, pp. 697–727, 1981.

[33] D. Harris, "The attenuation of electromagnetic waves due to atmospheric fog," *International Journal of Infrared and Millimeter Waves*, vol. 16, no. 6, pp. 1091–1108, 1995.

[34] N. C. Currie and C. E. Brown, Eds., *Principles and applications of millimeter wave radar*. Norwood: Artech House, 1987.

[35] J. Preissner, "The influence of the atmosphere on passive radiometric measurements," in *In AGARD Millimeter and Submillimeter Wave Propagation and Circuits 14 p*, 1979.

[36] International Telecommunication Union Radio Communication, "Specific rain attenuation model for rain for use in prediction models," *International Telecommunication Union*, 2005.

[37] ——, "Attenuation due to clouds and fog," *International Telecommunication Union*, 2013.

[38] I. I. Kim, B. McArthur, and E. J. Korevaar, "Comparison of laser beam propagation at 785 nm and 1550 nm in fog and haze for optical wireless communications," *Proc. SPIE*, vol. 4214, 2001.

[39] M. Al Naboulsi, H. Sizun, and Fornel, Fre de rique de, "Fog attenuation prediction for optical and infrared waves," *Optical Engineering*, vol. 43, no. 2, pp. 319–329, 2004.

[40] M. Zubair, Z. Haider, S. A. Khan, and J. Nasir, "Atmospheric influences on satellite communications," *Przeglad Elektrotechniczny*, vol. 87, no. 5, pp. 261–264, 2011.

[41] T. Oguchi, "Electromagnetic wave propagation and scattering in rain and other hydrometeors," *Proceedings of the IEEE*, vol. 71, no. 9, pp. 1029–1078, 1983.